XIII SIMMEC
Simpósio de Mecânica Computacional
29 de Outubro a 1º de Novembro de 2018
UFES - Campus Goiabeiras - Vitória, ES

ANÁLISE NUMÉRICA DE PROTEÇÕES PARA SENSORES DE FBG IMPRESSOS EM IMPRESSORAS 3D

Numerical Assessment of 3D Printed FBG Sensors Encapsulament

Natalia Reggiani Manzo (1) (P); Gabriel Teixeira Callado (2); Cristiano Monteiro de Barros Cordeiro (3); Luiz Carlos Marcos Vieira Junior (4)

(1) Engenheira Civil, Universidade Estadual de Campinas, Campinas - SP, Brasil.
(2) Estudante de Engenharia Física, Universidade Estadual de Campinas, Campinas - SP, Brasil.
(3) Dr. Prof., Universidade Estadual de Campinas, Campinas - SP, Brasil.
(4) Dr. Prof., Universidade Estadual de Campinas, Campinas - SP, Brasil.
Email para Correspondência: nataliarmanzo@gmail.com; (P) Apresentador

Resumo: Este trabalho tem como objetivo analisar numericamente a melhor configuração para uma proteção de sensores de fibra ótica baseados em redes de Bragg (FBG). Os sensores ópticos de FBG, uma nova tecnologia de medição, apresentam inúmeras aplicações na área de monitoramento de estruturas. O sensor ótico apresenta diversas vantagens em relação aos extensômetros com princípio de funcionamento elétrico. A fibra ótica desprotegida é muito frágil e, sem o encapsulamento, sua aplicação no monitoramento de estruturas torna-se impraticável. Atualmente, há proteções em desenvolvimento utilizando, principalmente, estruturas de manufatura complexa. Para esse trabalho, uma proteção produzida por impressão 3D foi estudada utilizando o software de elementos finitos ABAQUS (2016). A impressão 3D oferece liberdade na geometria de impressão das peças, o que permite a adaptação da proteção para monitoramento de estruturas com geometrias complexas. A proteção analisada nesse estudo foi desenvolvida para medição de deformação. Assim, inicialmente, modelou-se sólidos retangulares considerando os diferentes padrões de impressão. A peça foi submetida a tração a fim de verificar a distribuição de tensões e deformações. Após definir o melhor padrão de impressão, a proteção foi modelada em conjunto com um pórtico. Avaliou-se a influência do módulo de elasticidade da estrutura e a influência da espessura da peça na transferência da deformação para o sensor ótico. A análise em elementos finitos mostrou que, conforme o módulo de elasticidade da estrutura se aproxima do módulo de elasticidade do material da proteção, a rigidez da estrutura é alterada localmente. Da mesma maneira, a espessura da peça interfere na transferência da deformação. O fator de calibração aumenta de acordo com o aumento da espessura da peça e a distribuição de deformações na proteção é consideravelmente alterada. A influência do fator de preenchimento das proteções também foi estudada. Verificou-se que, proteções com menores fatores de preenchimento, apresentam menores fatores de calibração. O trabalho apresentado será complementado, em estudos futuros, com análises experimentais. Essa etapa é essencial para garantir a eficiência das proteções, uma vez que se assumiu simplificações nos modelos numéricos.

Palavras chaves: encapsulamento; sensores; FBG; simulação.

XIII SIMMEC
Simpósio de Mecânica Computacional
29 de Outubro a 1º de Novembro de 2018
UFES - Campus Goiabeiras - Vitória, ES

Abstract: This paper aims to numerically study the best design configuration for a Fiber Bragg Grating (FBG) Sensor packaging. FBG Sensors are new measuring technology that have been applied in structural health monitoring. It has numerous advantages over its electrical counterparts. The bare fiber optic, however, is very fragile and, without encapsulament, its application in structures become impractical. Nowadays, protection has been developed using, mainly, complex manufacturing structures. In this paper, a proposed 3D printed packaging is studied using finite element (FE) software ABAQUS (2016). 3D printing has the advantage to offer design freedom, which enables measurement of structures with complex configuration. The intended application for the FBG sensor, in this study, is to measure strain. As an initial analysis, a parallelepiped was modeled considering different printing patterns. A tension load was applied to assess the stress and strain distribution. After defining the best internal printing pattern, the protection was modelled combined with a frame. The packaging modulus of elasticity's influence on strain measurement and, the packaging thickness were evaluated. The FE analysis has showed that, as the modulus of elasticity of the structure approximates to the modulus of elasticity of the packaging material, it interferes locally with the structural stiffness, changing the strain results. The protection's thickness also interferes with the strain transferring. The thicker the protection, a higher a calibration factor must be used, and the strain distribution is reasonably changed. The packaging's filling percentages were also simulated, which was verified that lower filling percentages reduced the calibration factor. The paper presented herein will be complemented, in future studies, with the experimental analysis of packaging. This is essential to guarantee the packaging's efficiency, once simplifications were assumed in the numerical models.

Keywords: packaging; sensors; FBG; simulation.

1 INTRODUCTION

Structural health monitoring consists of continuously, or periodically, monitoring a structure during its life span. Information about several performance and structural condition parameters can be collected, according to the type of the structure, materials, loads, environmental conditions and expected damage being monitored (Glišić and Inaudi, 2007).

The great advantage of structural health monitoring is that monitoring a structure in a real-time basis during its entire lifetime allows adopting performance-based maintenance. Compared to scheduled and periodic maintenance, constant maintenance reduces costs and, increases structure reliability (Balageas et al., 2006). In addition, in the occasion of collapse, knowing the structure history of events facilitates its diagnosis; especially on complex structures that the structural behavior can hardly be defined analytically.

Structures are commonly assessed based on the mechanical stresses distribution and, the strength of the materials that compose the system. Stresses, however, cannot be directly measured on site. Therefore, strain must be measured and, with Hooke's Law, the stress is determined (Hoffmann, 1989).

Since its development, in 1938, electrical strain gauges have been widely used for strain data acquisition. Strain gauges are resistances, which values change due to the effects of mechanical stress. The resistance is an arm of a Wheatstone bridge circuit. Then, when the resistance changes, the bridge voltage becomes unbalanced and, the measurement is converted to strain (Hoffmann, 1989).

In the later years, optical fiber sensors have emerged as a new option in the measurement field. The major advantages of optical fibers over the electrical strain gauge are the immunity to electromagnetic interference and electrical noise, its multiplexing capability and, low loss transmission (Balageas et al., 2006).

As disadvantage, optical fibers can be very fragile. High shear stresses and curvatures can be critical for the bare optical fiber to break and loose signal (Glišić and Inaudi, 2007). Therefore, in order to apply optical fiber sensors in large scale, sensors packaging have been studied.

In this paper, a 3D printed packaging is studied. The 3D printer offers encapsulament design freedom and, can be easily manufactured. The best design configuration for packaging was studied numerically with the finite element software ABAQUS (2016). Additional numerical analyses were carried out to verify the influence of the modulus of elasticity of the substrate, and packaging on the strain transferring.

2 LITERATURE REVIEW

2.1 Optical Fiber

Optical fiber is a channel that carries a light beam through its length. The phenomenon of total internal reflection guides the light beam through the fiber. The optical fiber is composed

of a core, and cladding with refractive index slightly lower than the core. The cladding is important to guarantee that the signal will not be distorted (Thyagarajan and Ghatak, 2007).

Most common optical fibers present, both core and cladding, composed of pure silica. The core, however, is doped with germanium, which increases the refractive index of the core and guarantees the total internal reflection (Thyagarajan and Ghatak, 2007).

The optical fiber is mechanically protected by a very thin plastic coating, generally acrylate; high strength mechanical fibers and, a final external coating (Balageas et al., 2006). The bare optical fiber diameter is in the range of 125-500 μm (Glišić and Inaudi, 2007).

2.2 Fiber Bragg Grating (FBG)

Among the existing technologies for optical fiber sensors, there is the Fiber Bragg Gratings (FBG). Bragg gratings consists of exposing a short length of the fiber core to intense UV light, which will inscribe a periodic modulation of its refractive wavelength (Balageas et al., 2006; Glišić and Inaudi, 2007).

These alterations will behave like weak reflecting mirrors that, by accumulative wave interferences, will reflect back the wavelength corresponding to the grating spacing. All other wavelengths will be transmitted through the optical fiber undisturbed (Glišić and Inaudi, 2007).

The grating period is dependent of the strain and temperature, which allows the measurement of these properties with FBG sensors (Glišić and Inaudi, 2007). Subjecting the optical fiber to mechanical strain or temperature variation changes the grating period and, consequently, the reflected wavelength.

Equation (1) describes the relation between the change in the reflected wavelength and the strain for a FBG loaded axially (Othonos and Kalli, 1999). The formulation considers a simplification that the deformation in the transverse directions are proportional to the strain in the loaded direction, by the Poisson's ratio (Balageas et al., 2006).

$$\frac{\Delta\lambda}{\lambda_0} = (1 - p_e).\Delta\varepsilon \tag{1}$$

In which:

$\Delta\lambda$ - Wavelength shift
λ_0 - Inscribed wavelength
p_e - Photoelastic constant
$\Delta\varepsilon$ - Strain

The relation between the temperature and the reflected wavelength is given by Eq. (2) (Othonos and Kalli, 1999).

$$\frac{\Delta\lambda}{\lambda_0} = (\alpha + \zeta).\Delta T \tag{2}$$

In which:

$\Delta\lambda$ - Wavelength shift
λ_0 - Inscribed wavelength
α - Thermal expansion coefficient of silica
ζ - Thermo-optic coefficient
ΔT - Temperature variation

The FBG sensor is very stable to aging, once the sensor is the wavelength inscribed. Also, it has the multiplexing capability, which enables the measurement up to 16 different points with the same optical fiber (Balageas et al., 2006).

2.3 Sensor Packaging

As mentioned above, optical fibers are composed of silica, which is a brittle material. The coating provides the demanded mechanical strength for the fiber be easily handled. For the grating inscription, however, the bare optical fiber must be exposed to the UV light, becoming a critical breakage point (Maaskant et al., 1997).

Therefore, in order to guarantee FBG sensors applications in field, some packaging solutions have been developed in the later years. Leng et al. (2006) have developed several surface-mounted and embedded packaging systems based on metal and carbon fibre reinforced composite. Experimental tests on cylindrical concrete specimens were carried out, comparing strain results with electrical strain gauges.

Chung and Kang (2008) have embedded several FBG sensors in steel rebars of a full-scale railway bridge girder. A groove cut was made in the steel rebar, and the FBG were bonded with epoxy glue. Strain results were in good agreement with the acquired results from the electrical strain gauges.

Moyo et al. (2005) have developed a packaging system, in which the temperature effect can be compensated. The packaging consists of two FBG sensors; one is packaged in a metal tube, which protects the sensor from external stress, and the second is sandwiched between layers of carbon composite material. Thus, by the data acquisition of both sensors, the wavelength shift due to temperature is compensated. Experimental tensile tests presented results similar to electrical strain gauge.

Packaging developed in the papers above, although robust, present some manufacture complexity, and it is time consuming. Therefore, a simpler packaging is proposed in this paper using a basic 3D printer.

3 PACKAGING

The 3D printer model that will be used, in future studies, to print the packaging is Sethi3D AiP, which is a limited and affordable printer, in the range of existing 3D printers. PLA (Polyactic acid) filament, a plastic, was used for printing.

The packaging geometry is a rectangle of 1,0 cm x 2,5 cm and thickness of 0,32 cm. The thickness value was a limitation from the 3D Printer. Lower thickness generated pieces that were not uniform.

The FBG sensor is embedded in the packaging during printing. In the middle of the printing process, the printer is paused. The FBG sensor is positioned, prestressed and, then, the printing process is finished. Prestressing the FBG sensor is very important to guarantee the packaged sensors efficiency. Otherwise, the sensor might not measure the initial strains.

The 3D printer allows the input of different printing configurations. Between these setups, there are the printing pattern and, the filling percentage, that influence in the stress distribution. The 3D piece is generated printing layers in the z-direction. Each layer is printed following an internal geometric pattern, which available options for this printer model were: grid, triangular and, wiggle. These patterns create layers with voids, that present the geometry specified in the printing pattern. The size of the voids is controlled by the filling percentage. The lower the printing percentage, bigger the voids' size.

Then, due to their influence on the stress distribution, both configurations were decided carefully. The best printing pattern, and filling percentages of 100%, 80%, and 60% were studied.

4 NUMERICAL ANALYSIS

4.1 Printing Pattern Analysis

The printing pattern was chosen through an elastic linear numerical analysis in the finite element software ABAQUS (2016). The main objective was to observe the stress distribution in the different printing patterns. Therefore, rectangular pieces of 1,0 cm x 2,5 cm x 0,32 cm were modeled and, loaded longitudinally. The models with grid and triangular pattern are illustrated below.

a) Grid pattern model **b) Triangular pattern model**

Figure 1. Numerical Models.

The wiggle printing pattern was not modeled or considered for the packaging. Although this printing pattern has lines oriented to the load direction, which would generate a more uniform loading distribution, it also has void in this direction. Then, if poorly positioned, the

packaging would not be efficient because of the small contact area between the packaging and, the optical fiber.

For the simulation, a simplification was adopted. The printer prints the packaging by layers. Therefore, the bond between layers is not perfect. The models, however, did not consider it and, the pieces are modeled as a unique solid.

In the models, boundary conditions and loading were applied through a coupling constraint in the bottom and top surface. Then, the boundary conditions and loading were applied in reference points on the center of the surfaces. The displacements and rotations of the bottom surface were restrained in all directions. On the top surface, a tension load was applied. A first order analysis was carried out. The modulus of elasticity is based on the experimental characterization of the filament, and the Poisson's ratio is based on the values given by Farah et al. (2016).

The mesh was carefully studied. The mesh was varied until the displacements in the loading direction stabilizes. In the final mesh, a finer mesh was applied near the boundary conditions and loading. This enhanced the model analysis efficiency. The grid and triangular model presented, respectively, 102916 and 70323 elements. Solid element C3D8R from Abaqus library were used; this element is an eight-node hexahedral element with reduced integration and hourglass control. In the grid model, the hexahedral elements from the coarse mesh region have approximately the dimensions of 0,25 mm x 0,25 mm x 0,30 mm; and, in the finer mesh region, 0,15 mm x 0,15 mm x 0,30 mm. In the triangular model, the hexahedral elements from the coarse mesh region have approximately the dimensions of 0,40 mm x 0,40 mm x 0,30 mm; and, in the finer mesh region 0,15 mm x 0,15 mm x 0,30 mm.

The stress distribution for the model that simulates the grid pattern is shown in Figure 2. The stresses are according a local axis, which corresponds to the grid lines direction, and is a 45º rotation of the global axis. This coordinate system helps to observe that, if a bar element idealization is considered for the pattern, all the bars would be in tension. High positive stresses values and negative values can be noted in the legend. Those values, however, can only be verified on the surfaces that the boundary condition and loading are applied.

The strain in the longitudinal direction was also studied, once it is the property and direction that sensors measure. From Figure 3, it is possible to observe that the strain on the regions in which all the grid legs meet, differs from the strain in the grid legs. These points present the sum of the strain and stress of the grid legs. Therefore, it is expected that the resulting strain is different.

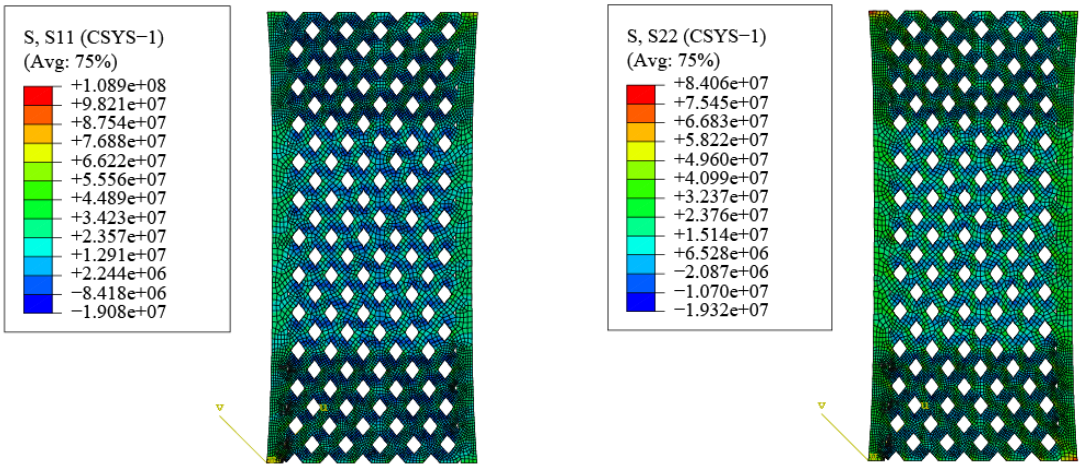

a) Stress distribution in local direction 1. **a) Stress distribution in local direction 2.**

Figure 2. Stress distribution for the grid printing pattern model.

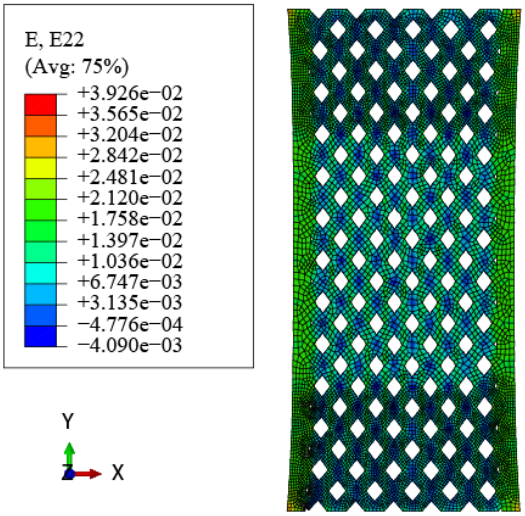

Figure 3. Strain distribution for the grid printing pattern in the longitudinal direction.

The stress distribution for the model that simulates the triangular pattern is shown in Figure 4. The elements oriented in the longitudinal direction carries most of the loading. Actually, if the triangular pattern is idealized as a truss system, no load is carried by the diagonals. In the strain distribution, however, it is still possible to notice different strain values in the region that the triangle diagonals meet, as shown in Figure 5.

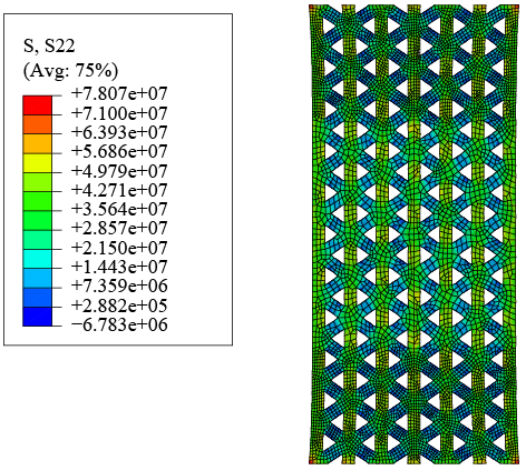

Figure 4. Stress distribution for the triangular printing pattern model.

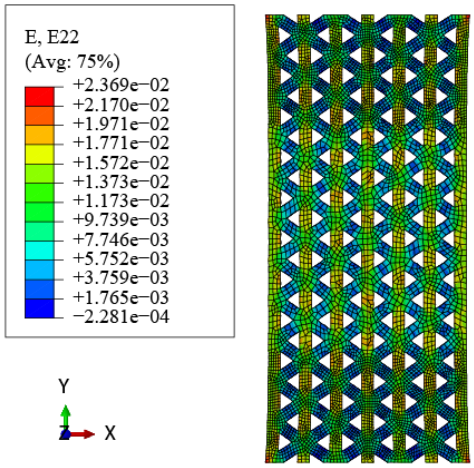

Figure 5. Strain distribution for the triangle printing pattern in the longitudinal direction.

In order to decide the best printing pattern, the strain, on the path the optical fiber is placed, was plotted. For both patterns, it was noticed that the strain varies along the path and, it presents a period in which the strain values repeat. Then, the average of this periodic strain variation was calculated, and compared with the global strain of the model. The global strain is the top displacement divided by the original length. The average of the periodic strain for the grid and triangular pattern model are, respectively, 0,2416% and 1,5186%. The global strains are 1,8837% and 1,5414%, respectively.

The FBG sensor is inscribed in a 4 mm length region of the optical fiber. There were two hypotheses for the strain measured by the sensor: (i) the strain only matters in the 4 mm region or; (ii) the global packaging deformation is important. The average of the periodic strain would represent the first hypothesis, and the global strain the other hypothesis.

The hypotheses could not be confirmed. Therefore, the triangular pattern, which presented closer values between the average and the global strain was preferred. Also, the stress being carried out mainly by the longitudinal direction was considered beneficial.

4.2 Frame-packaging interaction

The packaging, which dimensions were presented in Section 3, was modeled combined with the reduced-scale frame. The frame dimensions are presented in Figure 6. Three numerical models were considered, simulating the packaging printed with different filling percentage.

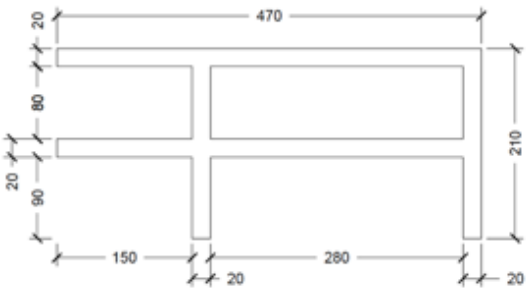

Figure 6. Frame Dimensions in mm.

The frame and packaging were modeled in the finite element software ABAQUS (2016). A pressure load was applied in both ends of the upper beam. The columns were considered perfectly encastred. The frame and packaging were modeled as solid elements. C3D8R element from Abaqus library was adopted. The mesh size was chosen in order to guarantee a similar proportion between all elements parts. The packaging has a finer mesh than the frame, in order to obtain more discretized results. The mesh size for the frame and the packaging is, respectively, 2,5 mm x 2,5 mm x 2,5 mm and, 0,625 mm x 0,625 mm x 0,40 mm.

A tie constraint was used to simulate the packaging and frame bonding. Packaging and frame present different mesh. According to Abaqus documentation (2016), however, mesh can be dissimilar in a surface-to-surface tie constraint.

The model's load distribution, boundary conditions, and dimensions, described above, were chosen because, in future studies, an experimental analysis will be carried out. And, the group have all the equipment and frames necessary to carry out the tests with these configurations.

The model's strain is evaluated in three paths. Figure 7 presents the strain along the paths for the packaging printed with 100% filling. The "Orig. Beam" corresponds to the expected strain, if the packaging was not introduced; "Strain Gauge" corresponds to strain next to the packaged, which would be the strain being measured by the strain gauge in the experimental analysis; and, the "Middle" corresponds to strain in the middle of packaging.

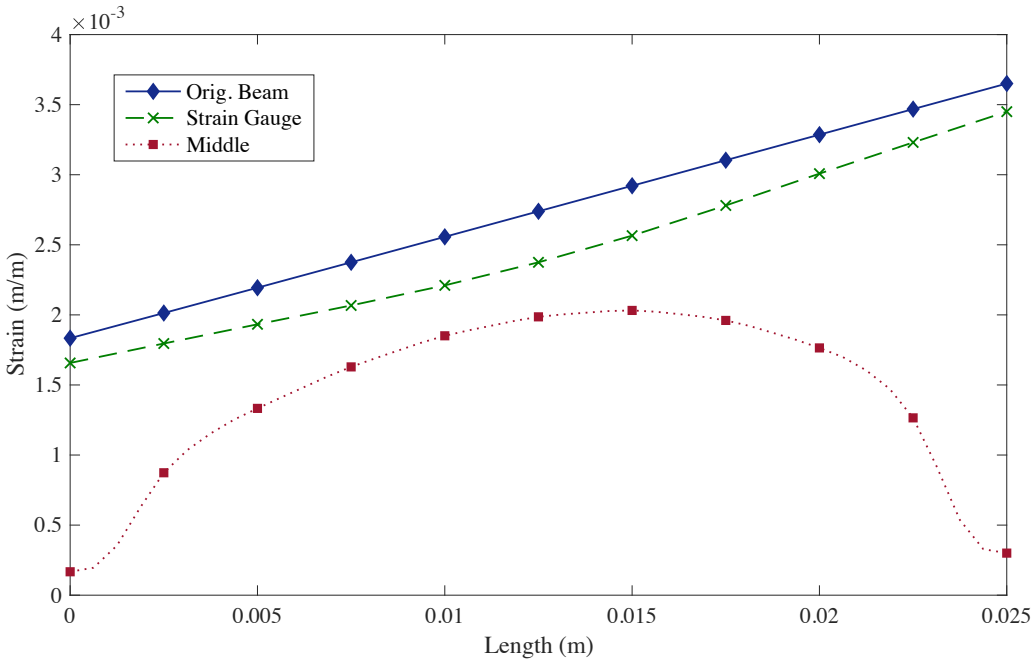

Figure 7. Strain along paths.

From the figure, it can be depicted that the strain on the middle of the packaging is reduced compared to the expected strain. This is due to the strain's transfer along the packaging height. In the middle path's ends, it is possible to note a drop on the strain. According to Hoffman (1989), this is due to a transition section, in which the strain is transferred from the frame to the packaging. Moreover, it can be verified that, although in smaller proportion, the packaging also influences on the strain gauge measurement.

The simulations with the packaging printed with 80% and 60% filling present strain similar to Figure 7. The curves' tendency is maintained, however, it is a curve with periodic variations. The strain periodic variation was expected, according to the numerical analysis of Section 4.1. In addition, the strain in the packaging printed with 80% and 60% filling approximate to the expected strain, considering the frame without the packaging.

In order to define a calibration factor based on the numerical data, it was considered that the sensors measured an average of the strain along the length that they are bonded. Therefore, the calibration factor was defined as the ratio of the average of the strain in the strain gauge path and, the average of the strain in the middle path.

Table 1 presents the calibration factor for the numerical analysis. It can be seen that it reduces, as the filling percentage is reduced. This is in agreement with the approximation of the strain curves to the expected strain diagram. As the voids increase, the packaging structure becomes more flexible, allowing the strain to be transferred.

Table 1. Calibration Factor for the numerical analysis.

Filling (%)	Calibration Factor
100	1,70
80	1,23
60	1,13

4.3 Packaging's Influence on the Frame

In the simulations, it was verified that the packaging influenced locally on the frame's strain. This behavior is generated by the composition of two factors. Primarily, the reduced-scale frame is composed of acrylic, which is a plastic. Then, the modulus of elasticity of the acrylic and filament are close, and the packaging influences on the frame strain. In addition, it is a reduced-scale model. The cross-section height of the frame beam is 2 cm. Introducing the packaging enhance the height in 16% and, consequently, the neutral axis shift can be significative. Therefore, in order to understand this influence, it was numerically evaluated.

The neutral axis shift was not considered on the numerical analysis. In real structure applications, the packaging height would be negligible to the structure cross-section height and, the neutral axis shift would also be negligible.

The modulus of elasticity's influence on the frame's strain was assessed by varying the modulus of elasticity of the frame on the numerical analysis. In addition, the analysis was carried out for packaging with lower thickness, in order to demonstrate that a more sophisticated printer would lead to better results. The error between the strain distribution of the frame model with and without the packaging is calculated by the standard root mean-squared error equation.

Figure 8 presents the modulus of elasticity's influence on the frame strain through the standard root mean-squared error (SRMSE) for different packaging thickness. It can be depicted that, as the frame's modulus of elasticity is more dissimilar to the packaging's modulus of elasticity, the strain is less influenced by the packaging. For concrete structures - which present modulus of elasticity around 25 GPa – with the packaging of 3,2 mm thickness, the error between the expected strain and the strain influenced by the packaging would be 5%, an acceptable error. For a metallic structure, this error would be even lower.

In addition, decreasing the packaging thickness would also be beneficial to reduce the packaging influence on the frame's strain. Packaging with 0,5 mm thickness would present an error lower than 10%, even with similar modulus of elasticity for the structure and packaging.

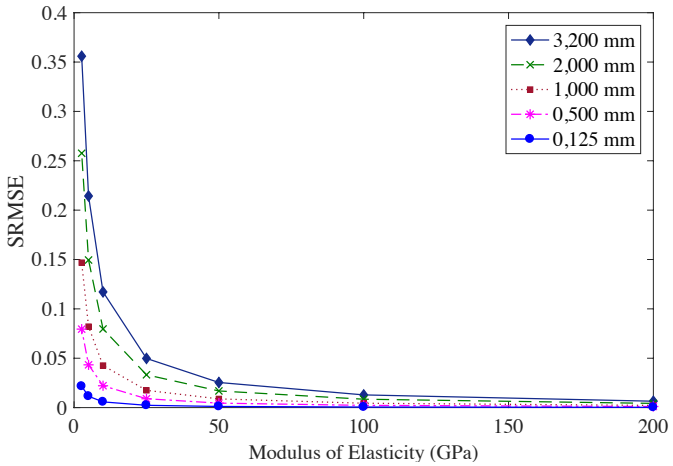

Figure 8. Packaging's influence on the frame's strain.

5 CONCLUSION

In this paper, a packaging design configuration for FBG sensors was studied. Considering the available printer and its configuration, the printing pattern, and filling percentage properties were evaluated. From the numerical analysis, the triangular printing pattern, among the other options, was chosen. The triangular printing pattern presented a more uniform stress distribution, as well as more coherent strain values between what was called global strain and, periodic strain variation.

The filling percentage was also studied numerically on the reduced-scale frames. The numerical analysis has shown that a smaller filling percentage would lead to strain closer to the strain measured by the electrical strain gauge, and consequently, smaller calibration factor.

Moreover, the analyses on the reduced-scale frames have shown that the strain measured by the packaged FBG sensor and the electrical strain gauge are influenced by the structure's modulus of elasticity and the packaging thickness. As the structure's modulus of elasticity differs more from the packaging's modulus of elasticity, the error between the sensors reduces. As well as, if the packaging thickness is reduced, the error will also reduce.

As next steps, in order to verify the hypotheses proposed herein based on the numerical analyses, these packaging will be studied experimentally. In the experiments, some numerical simplifications have to be checked. For instance, the perfect bond between the packaging and the frame.

ACKNOWLODGMENTS

The group would like to thank the support of The Sao Paulo Research Foundation (FAPESP) for the grating conceded under the grant number 16/23408-3, and to the Center of Petroleum Studies (CEPETRO) for the grating under the process number 2014/00090-2.

REFERENCES

ASTM D638-14, 2014. *Standard Test Method for Tensile Properties of Plastics*. West Conshohocken, PA: ASTM International.

Balageas, D., Fritzen C., & Güemes, A. (Eds.), 2006. *Structural Health Monitoring*. Newport Beach, CA: ISTE Ltd.

Chung, W., & Kang, D., 2008. *Full-scale test of a concrete box girder using FBG sensing system*. Engineering Structures, vol. 30, pp. 643-652.

Farah, S., Anderson, D., & Langer, R., 2016. *Physical and mechanical properties of PLA, and their functions in widespread applications – A comprehensive review*. Advanced Drug Delivery Reviews.

Glišić, B., & Inaudi, D., 2007. *Fibre Optic Methods for Structural Health Monitoring*. Chichester, UK: John Wiley Sons & Ltd.

Hoffman, K., 1989. *An Introduction to Measurements using Strain Gages*. Alsback, Germany: Hottinger Baldwin Messtechnik GmbH.

Leng, J. S., Barnes, R. A., Hameed, A., Winter, D., Tetlow, J., Mays, G.C., & Fernando, G.F., 2006. *Structural NDE of concrete structures using protected EFPI and FBG sensors*. Sensors and Actuators A, vol. 126, pp. 340-347.

Moyo, P., Brownjohn, J. M. W., Suresh, R., Tjin, S. C., 2005. *Development of fiber Bragg grating sensors for monitoring civil infrastructure*. Engineering Structures, vol. 27, pp. 1828-1834.

Maaskant, R., Alavie, T., Measures, R. M., Tadros, G., Rizkalla, S. H., & Guha-Thakurta, A., (1997). *Fiber-optic Bragg Grating Sensors for Bridge Monitoring*. Cement and Concrete Composites, vol. 19, pp. 21-33.

Othonos, A., Kalli, K., 2000. *Fiber Bragg Gratings: Fundamentals and Applications in Telecommunications and Sensing*. Corning, NY: Corning Incorporated.

Smith, M., 2016. *Abaqus Documentation*. Providence, RI: Simulia.

Thyagarajan, K., & Ghatak, A., 2007. *Fiber Optic Essentials*. Hoboken, NJ: John Wiley & Sons, Inc.